Physical insights into inverse-scattering profiles and symmetric dispersionless FBG designs

Michalis N. Zervas,[1,2,*] and Michael K. Durkin,[2]

[1]*Optoelectronics Research Centre, University of Southampton, Southampton SO17 1BJ, UK*
[2]*SPI Wellington Park, Tollbar Way, Hedge End, Southampton SO30 2QU, UK*
[*]*mnz@orc.soton.ac.uk*

Abstract: We revisit representative and widely used inverse-scattering fiber Bragg grating designs and shed physical insight into their characteristics. We first demonstrate numerically and experimentally that dispersionless square filters are actually dispersion compensated devices and we physically identify the spatially separated main (dispersive) reflector and dispersion compensator sections. We also look into the features of pure 2nd-order dispersion and 3rd-order dispersion compensator designs and discuss their physical importance. Finally, we use the gained physical insight to design strong symmetric gratings with dispersionless response from both sides. Using this knowledge we design and fabricate strong (>30dB) bidirectional dispersionless filters.

OCIS codes: (050.2770) Gratings; (060.3735) Fiber Bragg gratings; (230.1480) Bragg reflectors; (260.2030) Dispersion.

References and links

1. K. O. Hill, Y. Fujii, D. C. Johnson, and B. S. Kawasaki, "Photosensitivity in optical waveguides: application to reflection filter fabrication," Appl. Phys. Lett. **32**(10), 647–649 (1978).
2. C. R. Giles, "Lightwave applications of fiber Bragg gratings," J. Lightwave Technol. **15**(8), 1391–1404 (1997).
3. A. Othonos and K. Kalli, *Fiber Bragg Gratings: Fundamentals and Applications in Telecommunications and Sensing*, Artech House Inc. (1999).
4. R. I. Laming, N. Robinson, P. L. Scrivener, M. N. Zervas, S. Barcelos, L. Reekie, and J. A. Tucknott, "A dispersion tunable grating in a 10-Gb/s 100-220 km step-index fiber link," IEEE Photon. Technol. Lett. **8**(3), 428–430 (1996).
5. Y. Painchaud, M. Lapointe, F. Trépanier, R. L. Lachance, C. Paquet, and M. Guy, "Recent Progress on FBG-Based Tunable Dispersion Compensators for 40 Gb/s Applications," Proc. Optical Fiber Commun./National Fiber Optic Engineers Conf. (OFC/NFOEC '07) (Anaheim, CA, 2007), paper OThP3.
6. T. Schmidt, C. Malouin, R. Saunders, J. Hong, and R. Marcoccia, "Mitigating channel impairments in high capacity serial 40G and 100G DWDM transmission systems," IEEE/LEOS Summer Topical Meetings, ME2.2, 141–142 (2008).
7. G. Raybon, P. J. Winzer, H. Song, A. Adamiecki, S. Corteselli, A. H. Gnauck, T. Kissell, D. A. Fishman, N. M. Denkin, Y.-H. Kao, T. L. Downs, A. Carenza, S. Scrudato, E. H. Goode, W. A. Thompson, C. R. Doerr, L. L. Buhl, T. Xia, G. Wellbrock, W. Lee, G. Lyons, P. Hofmann, T. T. Fisk, E. B. Basch, W. J. Kluge, J. R. Gatewood, T. Kawanishi, K. Higuma, and Y. Painchaud, "100 Gb/s DQPSK Field Trial: Live Video Transmission Over an Operating LambdaXtreme® Network," Bell Lab. Tech. J. **14**(4), 85–113 (2010).
8. A. Galvanauskas, M. E. Fermann, D. Harter, K. Sugden, and I. Bennion, "All-fiber femtosecond pulse amplification circuit using chirped Bragg gratings," Appl. Phys. Lett. **66**(9), 1053–1055 (1995).
9. R. Gumenyuk, I. Vartiainen, H. Tuovinen, and O. G. Okhotnikov, "Dissipative dispersion-managed soliton 2 μm thulium/holmium fiber laser," Opt. Lett. **36**(5), 609–611 (2011).
10. D. C. Adler, W. Wieser, F. Trepanier, J. M. Schmitt, and R. A. Huber, "Coherence length extension of Fourier domain mode locked lasers," Proc. SPIE **8213**, 82130O, 82130O-4 (2012).
11. M. Ibsen, R. Feced, P. C. Teh, J. H. Lee, M. R. Mokhtar, P. Petropoulos, M. N. Zervas, D. J. Richardson, and D. N. Payne, "Advanced Bragg grating devices and where they are going," Proc. 27th Australian Conference on Optical Fibre Technology (ACOFT), 89–91 Sydney (2002).
12. M. Ibsen and R. Feced, "Fiber Bragg gratings for pure dispersion-slope compensation," Opt. Lett. **28**(12), 980–982 (2003).
13. H. A. Haus, J. D. Moores, and L. E. Nelson, "Effect of third-order dispersion on passive mode locking," Opt. Lett. **18**(1), 51–53 (1993).

#190362 - $15.00 USD Received 10 May 2013; revised 4 Jul 2013; accepted 5 Jul 2013; published 15 Jul 2013

14. M. L. Dennis and I. N. Duling III, "Third-order dispersion in femtosecond fiber lasers," Opt. Lett. **19**(21), 1750–1752 (1994).
15. G. Meltz, W. W. Morey, and W. H. Glenn, "Formation of Bragg gratings in optical fibers by a transverse holographic method," Opt. Lett. **14**(15), 823–825 (1989).
16. S. J. Mihailov, C. W. Smelser, P. Lu, R. B. Walker, D. Grobnic, H. Ding, G. Henderson, and J. Unruh, "Fiber Bragg gratings made with a phase mask and 800-nm femtosecond radiation," Opt. Lett. **28**(12), 995–997 (2003).
17. H. Kogelnik, "Filter response of nonuniform almost-periodic structures," Bell Syst. Tech. J. **55**, 109–126 (1976).
18. P. St. J. Russell, T. A. Birks, and F. D. Lloyd-Lucas, "Photonic Bloch waves and photonic band gaps," in Confined Electrons and Photons, E. Burnstein, C. Weisbuch (Eds), 585–633, Plenum (1995).
19. H. Kogelnik and C. V. Shank, "Coupled-wave theory of distributed feedback lasers," J. Appl. Phys. **43**(5), 2327–2335 (1972).
20. M. Yamada and K. Sakuda, "Analysis of almost-periodic distributed feedback slab waveguides via a fundamental matrix approach," Appl. Opt. **26**(16), 3474–3478 (1987).
21. P. S. Cross and H. Kogelnik, "Sidelobe suppression in corrugated-waveguide filters," Opt. Lett. **1**(1), 43–45 (1977).
22. K. Ennser, M. N. Zervas, and R. I. Laming, "Optimization of apodized linearly chirped fiber gratings for optical communications," IEEE J. Quantum Electron. **34**(5), 770–778 (1998).
23. K. A. Winick and J. E. Roman, "Design of corrugated waveguide filters by Fourier-transform techniques," IEEE J. Quantum Electron. **26**(11), 1918–1929 (1990).
24. G. L. Lamb, Jr., "Elements of soliton theory," New York: Wiley (1980).
25. A. M. Bruckstein, B. C. Levy, and T. Kailath, "Differential methods in inverse scattering," SIAM J. Appl. Math. **45**(2), 312–335 (1985).
26. R. Feced, M. N. Zervas, and M. A. Muriel, "An efficient inverse scattering algorithm for the design of nonuniform fiber Bragg gratings," IEEE J. Quantum Electron. **35**(8), 1105–1115 (1999).
27. J. Skaar, L. Wang, and T. Erdogan, "On the synthesis of fiber Bragg gratings by layer peeling," J. Quantum Electron. **37**(2), 165–173 (2001).
28. A. Rosenthal and M. Horowitz, "New technique to accurately interpolate the complex reflection spectrum of fiber Bragg gratings," IEEE J. Quantum Electron. **40**(8), 1099–1104 (2004).
29. L. Huang, W. Huang, J. Wang, and G. Yang, "Improved layer peeling algorithm for strongly reflecting fiber gratings," Chin. Opt. Lett. **4**, 505–507 (2006).
30. M. Ibsen, R. Feced, P. Petropoulos, and M.N. Zervas, "99.9% reflectivity dispersion-less square-filter fibre Bragg gratings for high speed DWDM networks," in Proceedings of Optical Fiber Communications Conference, paper PD21 (2002).
31. K. H. Ylä-Jarkko, M. N. Zervas, M. K. Durkin, I. Barry, and A. B. Grudinin, "Power Penalties Due to In-Band and Out-of-Band Dispersion in FBG Cascades," J. Lightwave Technol. **21**(2), 506–510 (2003).
32. M. K. Durkin and M. N. Zervas, "Apparatus for filtering optical radiation at an operating wavelength," Patent No: US6,947,641 (2005).
33. P. Minzioni and M. Tormen, "Bragg gratings: Impact of apodization lobes and design of a dispersionless optical filter," J. Lightwave Technol. **24**(1), 605–611 (2006).
34. M. N. Zervas and M. K. Durkin, "Physical insight into dispersionless FBG designs," in Bragg Gratings, Photosensitivity, and Poling (BGPP) in Glass Waveguides, paper BM3D.6, Colorado (2012).
35. M. J. Cole, W. H. Loh, R. I. Laming, M. N. Zervas, and S. Barcelos, "Moving fibre/phase mask-scanning beam technique for enhanced flexibility in producing fibre gratings with a uniform phase mask," Electron. Lett. **31**(17), 1488–1490 (1995).
36. W. H. Loh, M. J. Cole, M. N. Zervas, S. Barcelos, and R. I. Laming, "Complex grating structures with uniform phase masks based on the moving fiber-scanning beam technique," Opt. Lett. **20**(20), 2051–2053 (1995).
37. C. Riziotis and M. N. Zervas, "Effect of in-band group delay ripple on WDM filter performance," 27th European Conf. Opt. Commun. **4**, 492–493 (2001) (ECOC).
38. M. Sumetsky, B. J. Eggleton, and C. de Sterke, "Theory of group delay ripple generated by chirped fiber gratings," Opt. Express **10**(7), 332–340 (2002).
39. M. K. Durkin, R. Feced, C. Ramirez, and M. N. Zervas, "Advanced fibre Bragg gratings for high performance dispersion compensation in DWDM systems", Optical Fiber Communications Conf. **1**, 121–123 (2000).
40. K. Ennser, M. Ibsen, M. Durkin, M. N. Zervas, and R. I. Laming, "Influence of non-ideal chirped fiber grating characteristics on dispersion cancellation," IEEE Photon. Technol. Lett. **10**(10), 1476–1478 (1998).
41. F. Knappe, H. Renner, and E. Brinkmeyer, "Efficient design of spatially symmetric Bragg gratings for add/drop multiplexers," AEU Int. J. Electron. Commun. **62**(7), 513–520 (2008) (AEÜ).
42. A. V. Nemykin and D. A. Shapiro, "Optical FBG filter with minimum group delay for WDM systems," Opt. Commun. **289**, 97–102 (2013).

1. Introduction

Since their first demonstration in 1978 [1], fiber Bragg gratings (FBGs) have found widespread usage in lab experiments and a plethora of applications across the photonics domain [2,3]. Their versatility stems from the ability to control very accurately their

#190362 - $15.00 USD Received 10 May 2013; revised 4 Jul 2013; accepted 5 Jul 2013; published 15 Jul 2013

reflection and dispersion characteristics by proper design. Linearly-chirped FBGs have been used extensively over the years for 2nd-order dispersion compensation in optical communication transmission systems [4,5]. Even with the current effectiveness of electronic dispersion compensation, FBG-based linear dispersion compensators are expected to continue to play a role in hybrid compensation schemes in future high speed optical systems [6,7]. In addition, linearly chirped FBG have been extensively used for pulse stretching and re-compression in chirped-pulse amplification high power fiber laser systems [8]. Lately, linearly-chirped FBGs have also been used to provide normal total dispersion in dissipative dispersion-managed soliton mid-IR fiber laser systems, where fibers with normal dispersion do not exist [9]. They can also provide broadband dispersion compensation for the development of Fourier-domain mode-locked fiber lasers for long-range optical coherence tomography [10]. Pure 3rd-order dispersion compensation FBGs [11,12], on the other hand, can be potentially used for dispersion trimming in optical telecommunication systems and transform-limited ultrashort-pulse fiber lasers [13,14].

FBGs are in general quasi-periodic structures written permanently inside the fiber core using appropriate CW UV exposure [15] or more recently fs near-IR laser irradiation [16]. Fiber Bragg gratings are generally characterized by a refractive index variation given by:

$$n(z) = n_0 + \Delta n(z)\cos\left[K_0 z + \varphi(z)\right] \tag{1}$$

where n_0 is the background refractive index, $\Delta n(z)$ is the amplitude distribution of the perturbation (apodization or refractive index modulation profile), $\varphi(z)$ is the phase variation of the perturbation, and $K_0 = 2\pi/\Lambda_0$ where Λ_0 is a reference period. The spatial phase variation $\varphi(z)$ corresponds to an equivalent local period detuning or chirp given by [17]:

$$\Delta\Lambda(z) = -\frac{\Lambda_0^2}{2\pi}\frac{d\varphi}{dz} \tag{2}$$

The local period distribution is $\Lambda(z) = \Lambda_0 + \Delta\Lambda(z)$. The refractive index distribution of Eq. (1) is equivalent to a generalized coupling constant:

$$q(z) = q_0(z)e^{-i\varphi(z)} \tag{3}$$

where $q_0(z) = -i(\pi/\lambda_0)\Delta n_0(z)$ and $\lambda_0 = 2n_0\Lambda_0$. Given the refractive index distribution $n(z)$ or equivalent coupling constant $q(z)$, the FBG *analysis* consists in deriving the reflection coefficient:

$$r(\lambda) = r_0(\lambda)e^{i\theta(\lambda)} \tag{4}$$

where $r_0(\lambda)$ is the reflection coefficient magnitude and $\theta(\lambda)$ the reflection phase. The latter is associated with the relative group delay by:

$$\Delta\tau(\lambda) = \frac{\partial\theta}{\partial\omega} = -\frac{n_0\lambda_0^2}{2\pi c}\frac{d\theta}{d\lambda} \tag{5}$$

A number of methods, including Bloch modes [18], coupled-mode theory [19] or transfer-matrix method [20], can be used for the analysis of general FBGs. In order to achieve optimum performance, in most applications the FBG main parameters, i.e. local strength and period detuning, should be tailored appropriately. Traditionally, improved designs were obtained by applying suitable apodization to both ends of otherwise uniform structures [21,22]. In most of these cases, however, the improvement on one characteristic, e.g. dispersion linearity, was usually achieved at the expense of another parameter, e.g. bandwidth utilization.

In optimizing the filter response, a number of different refractive index profiles or coupling constants are considered and their impact on the FBG performance is evaluated

#190362 - $15.00 USD Received 10 May 2013; revised 4 Jul 2013; accepted 5 Jul 2013; published 15 Jul 2013

against certain criteria. A much more efficient approach, however, is to use direct *synthesis* or *inverse scattering* (IS) of the required FBG [see Fig. 1)]. This consists in defining first the required reflection coefficient or impulse response and work backwards to define the corresponding generalized coupling constant $q(z)$ or refractive index distribution $n(z)$ and local detuning $\Delta\Lambda(z)$. A number of methods can be used for this purpose including Fourier Transforms [23], Integral [24] or Differential IS methods [25].

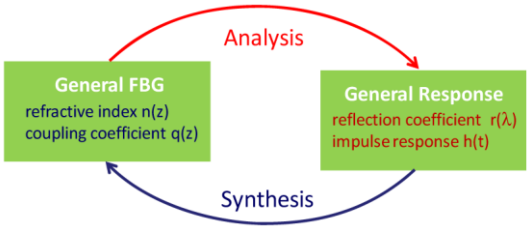

Fig. 1. General FBG analysis and synthesis schematic

FBG device effectiveness took a leap forward with the introduction of efficient IS design algorithms. Such advanced approaches allowed a number of FBG performance characteristics to be optimized simultaneously. Layer-peeling, in particular, has been established as a major design algorithm for advanced grating-based devices [26–29]. Starting from the required optimum transfer function and applying causality, the required refractive-index modulation and chirp profile are obtained. The freedom to choose arbitrarily the response though comes at the expense of device complexity. IS algorithms usually result in intricate designs that depart considerably from established intuitive and straightforward configurations. A typical example is the multi-lobe FBG design with square dispersionless response, which enables dense wavelength-division-multiplexing (WDM) [30] and large number of concatenated add-drop functions without substantial penalty [31]. However, such gratings are uni-directional and cannot be used from both sides, which severely compromises their use as add *AND* drop multiplexers. Other examples include pure 2nd- or 3rd-order dispersion compensators, as will be discussed in this work.

So far in the literature emphasis has been placed primarily on the accuracy of the IS mathematical formulations and no attempt has been made to physically understand how these otherwise mathematically rigorous designs really work. In this paper, we revisit some of the most successful IS FBG designs and shed physical insight into their characteristics. We first demonstrate numerically and experimentally that dispersionless square filters are actually *dispersion compensated* devices and we physically identify the spatially separated *main (dispersive) reflector* and *dispersion compensator* sections. We also look into the features of pure 2nd- and 3rd-order dispersion compensator designs and discuss their physical importance. Finally, we use the gained physical insight to design strong symmetric gratings with dispersionless response from both sides.

2. Physical Insight into Inverse-Scattering FBG Designs

In this section we consider specific examples of dispersion-engineered optical devices based on IS FBG designs. The details of the layer-peeling IS design algorithms are well described in the literature [26–29] and are not repeated here. The interested readers can refer to these papers to acquaint themselves with the mathematical details. Any of these formulations can be used for the design resulting in FBG profiles with similar features. In this work we concentrate primarily on the physical significance of the designs. The desired reflection coefficient is generally given by:

#190362 - $15.00 USD Received 10 May 2013; revised 4 Jul 2013; accepted 5 Jul 2013; published 15 Jul 2013

$$r(\Delta\lambda) = \sqrt{R_0}\exp\left[\left(2\frac{\Delta\lambda}{\Delta\lambda_0}\right)^{2m}\right]\exp\left[+i\Delta\theta(\lambda)\right] \tag{6}$$

where R_0 is the peak reflectivity, λ_0 is the center wavelength, $\Delta\lambda = (\lambda - \lambda_0)$ is the wavelength detuning and $\Delta\lambda_0$ is the filter bandwidth. The integer m in the exponent of the super-Gaussian profile defines the "squareness" of the reflection spectrum. The reflection phase is generally given by:

$$\theta(\Delta\lambda) = -\frac{2\pi c}{\lambda_0^2}\int \Delta\tau(\lambda)d\Delta\lambda \tag{7}$$

where

$$\Delta\tau(\Delta\lambda) = \Delta\tau_{ref} + D_2\Delta\lambda + D_3\Delta\lambda^2 \tag{8}$$

and

$$\Delta\tau_{ref} = n_0 L_0 / c \tag{9}$$

is a reference time delay used to make the transfer function in Eq. (6) causal. D_2 and D_3 define the 2nd- and 3rd-order dispersion, respectively.

2.1: Linear-Phase (Dispersionless) FBG Filters ($D_2 = D_3 = 0$)

The reflection coefficient of a square linear-phase (dispersionless) grating is obtained by setting $D_2 = D_3 = 0$ in Eq. (8).

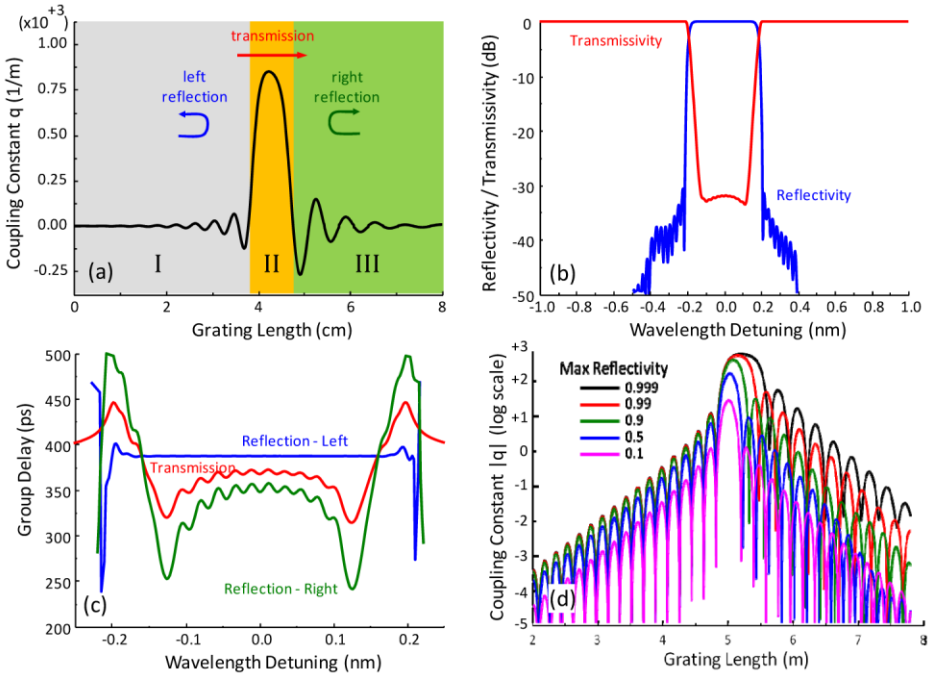

Fig. 2. Dispersionless FBG characteristics: (a) Coupling constant (b) reflectivity & transmissivity and (c) reflection (left & right) and transmission group delays, (d) coupling constant (log scale) for varying reflectivity.

#190362 - $15.00 USD Received 10 May 2013; revised 4 Jul 2013; accepted 5 Jul 2013; published 15 Jul 2013

Figure 2(a) shows the coupling constant distribution for a square dispersionless FBG filter with R_0 = 0.9995, $\Delta\lambda_0$ = 0.4nm and m = 22. The coupling constant and the associated RI modulation profile is highly asymmetric. It consists of a main lobe (II) preceded and followed by secondary lobe series I & III of different heights and periodicity. Figure 2(b) shows the reflectivity and transmissivity spectra, while Fig. 2(c) shows the reflection group delay from left and right. It is evident that the filter is dispersionless only when light enters from the left. The reflection from the opposite side, on the other hand, is highly dispersive. This obviously compromises severely the ability to accomplish add *and* drop function by the same FBG. As in all FBGs, the group delay in transmission is the average of the two reflection group delays. The negative coupling constant is achieved by inserting π-phase shifts at the zero crossing points. Figure 2(d) plots the coupling constant (in log scale, in order to reveal small features) with varying peak reflectivity R_0. It is shown that the coupling constant and, therefore, the associated RI distribution becomes progressively more asymmetric as the reflectivity is increased. It is observed that the periodicity of section I remains constant, while the size of section II and the periodicity of section III increase with R_0. It should also be mentioned that the RI distribution is symmetric only for $R_0 \leq 0.1$.

Following this analysis, we can consider the complex RI modulation profiles of the dispersionless IS designs as consisting of two distinct parts, denoted as front and back parts. The front part comprises only the constant period preceding lobe series (section I). The back part, on the other hand, comprises the main lobe (section II) and the following lobe series (section III) [32–34]. We will show that these distinct parts, in addition to developing differently with increasing the peak reflectivity, contribute in different ways to the FBG overall reflectivity and dispersion.

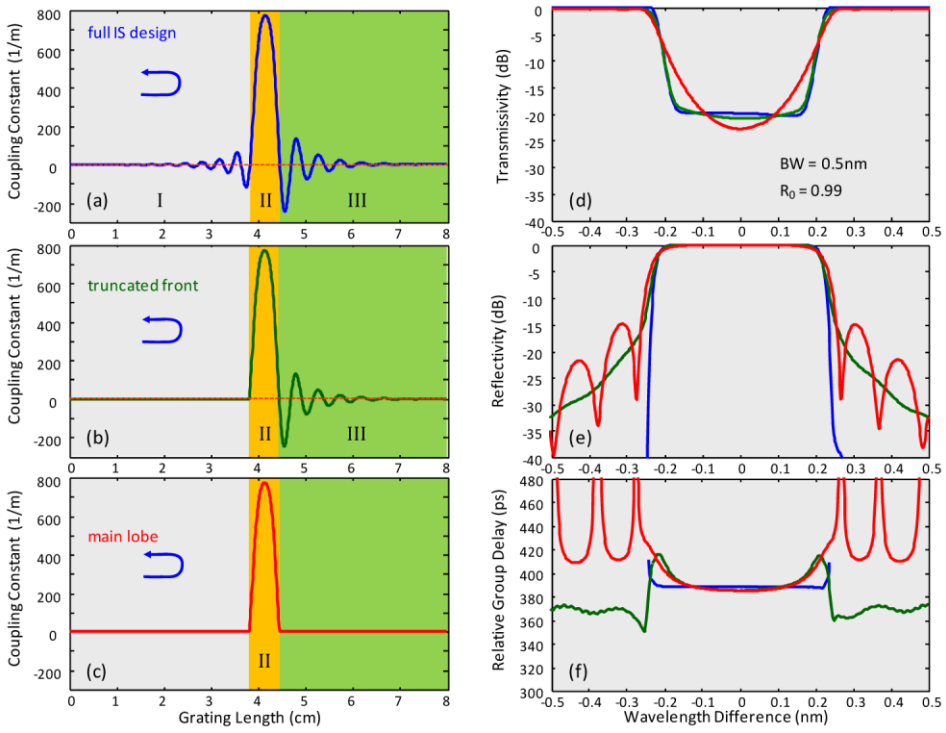

Fig. 3. Dispersionless IS FBG design (a) full coupling constant distribution (regions I + II + III), (b) truncated profiles II + III and (c) central lobe II. (d)-(f) show the corresponding transmissivities, reflectivities and group delays.

#190362 - $15.00 USD Received 10 May 2013; revised 4 Jul 2013; accepted 5 Jul 2013; published 15 Jul 2013

Figure 3(a) shows the full distribution (regions I + II + III) of the coupling constant for a dispersionless FBG, with $R_0 = 0.99$, $\Delta\lambda_0 = 0.5$nm and $m = 22$. Figure 3(b) and 3(c) show the truncated profiles (sections II + III) and the central lobe (section II), respectively. Figure 3(d)-3(f) show the corresponding transmissivities, reflectivities and group delays, respectively. Compared to the full profile [Fig. 3(a) and blue lines], it is observed that truncating the front section I [Fig. 3(b) and green lines] results in minimum changes in the "squareness" of the transmissivity and reflectivity (the reflectivity is affected mostly below the –25dB level). In contrast, the effect on the group delay is much more pronounced. These results show that the front section I controls the group delay flatness. In other words, section I acts primarily as the "*dispersion compensator*" of the full IS FBG design. Finally, truncating section III and retaining lobe II only [Fig. 3(c) and red lines] results in a "non-square" transmission spectrum. In addition, typical side-lobes appear in the reflectivity spectrum, while there is no additional penalty in the group delay spectrum. It is then deduced that section III controls primarily the transmissivity "squareness" by reducing the transmission around the spectrum center and increasing it at the spectrum edges. Section III works primarily as "spectrum modifier" and does not affect the overall dispersion. The functionality of the different FBG parts has not been discussed before.

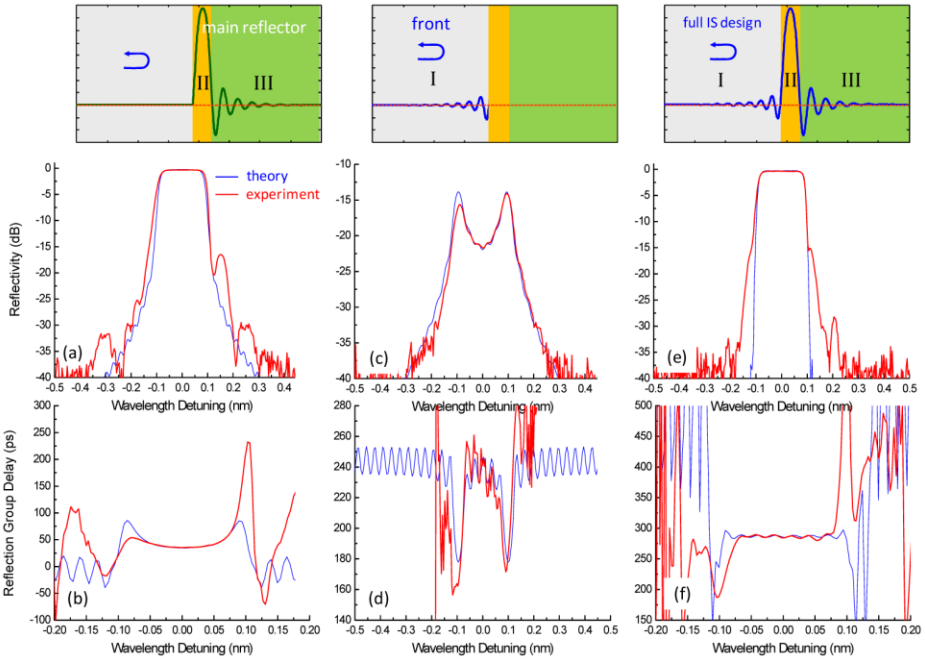

Fig. 4. Inverse scattering dispersionless FBGs; Reflectivity and Group Delay spectra for (a)&(b) main reflector (sections II + III), (c)&(d) dispersion compensator (section I) and (e)&(f) entire grating (I + II + III), (blue lines: theory, red lines: experiment).

To explore further the identified IS FBG design features, three different gratings, consisting of front part (section I), back part (II + III) and whole dispersionless FBG (I + II + III), were written using a modified "moving fiber-scanning beam" technique [35,36] and measured separately. Figure 4(a) and 4(b) show the reflectivity and reflection group delay, respectively, of the back part (II + III) alone. In agreement with previous observations, this part provides strong reflection and it is highly dispersive. Figure 4(c) and 4(d) show the reflectivity and group delay, respectively, of the front part (section I) alone. The front part provides negligible reflection and it is again highly dispersive with dispersion, however, of opposite sign to the front part. Figure 4(e) and 4(f) finally show the reflectivity and group

#190362 - $15.00 USD Received 10 May 2013; revised 4 Jul 2013; accepted 5 Jul 2013; published 15 Jul 2013

delay, respectively, of the whole FBG. Its reflectivity is shown to be largely the same with the one of the front part while its group delay is substantially flattened. The residual ripple is of small enough magnitude and period to cause any substantial penalty to high bit-rate data [37]. Figure 4(a)-4(d) include both the theoretical (blue lines) and experimental (red lines) results, showing very good agreement. The small discrepancy is due to slight inaccuracies in the amount of π-phase shifts required for the dispersionless IS designs.

2.2 Pure 2nd-Order Dispersion Compensators ($D_2 \neq 0$, $D_3 = 0$)

Layer-peeling IS algorithms are again the preferred design approach for fabrication of high performance FBG-based pure 2nd-order dispersion compensators. The reflection coefficient of a linear dispersion compensator defined by setting $D_2 \neq 0$ and $D_3 = 0$ in Eq. (8).

As in the case of dispersionless FBGs, IS-based designs for 2nd-order dispersion compensators are complex with non-intuitive features. Figure 5(a) shows schematically the design reflectivity and time-delay spectrum of a 2nd-order dispersion compensating FBG. The parameters used were $R_0 = 0.99$, $\Delta\lambda_0 = 0.6$nm, $m = 120$ and $D_2 = 1500$ps/nm. Figure 5(b) shows the apodization profile (coupling constant distribution) and chirp (local detuning) of the layer-peeling IS design. It is evident that both the apodization and local detuning variations are complex and departing considerably from standard and intuitive profiles used extensively in the past in order to minimize in-band group delay ripples [22]. Figure 5(c), on the other hand, shows the apodization profile (coupling constant) and local period detuning (chirp) distributions of a conventional, linearly-chirped FBG. The FBG total length is 18cm and the applied local period detuning is 0.2nm. The apodization profile is a super-gaussian function with exponent $m = 120$, $L_0 = 18$cm and maximum coupling constant of 172m^{-1}. Figure 5(d) shows the resulting reflectivity and group-delay spectra of such grating. Despite the slight apodization, the reflectivity spectrum is undulating. In addition, the group delay shows strong ripples over the reflection bandwidth.

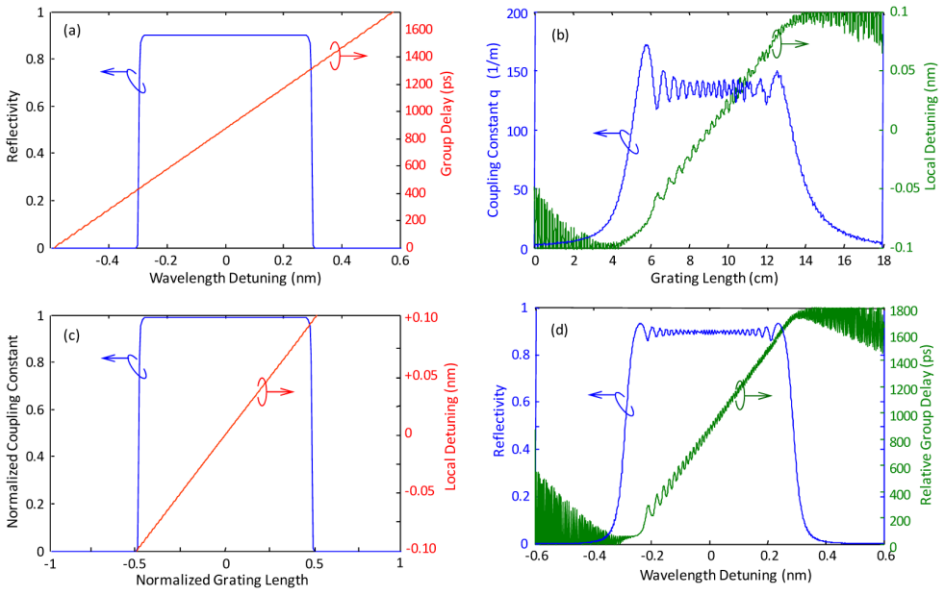

Fig. 5. Reflectivity and group-delay spectrum of a 2nd-order dispersion compensating FBG ($R_0 = 0.99$, $\Delta\lambda_0 = 0.6$nm, $m = 120$ and $D_2 = 1500$ps/nm), (b apodization profile (coupling constant) and chirp (local detuning) of the layer-peeling IS design, (c) apodization profile (coupling constant) and local period detuning (chirp) distributions of a conventional, linearly-chirped FBG. The FBG total length is 18cm and the applied local period detuning is 0.2nm. The apodization profile is a super-gaussian function with exponent $m = 120$, $L_0 = 18$cm and maximum coupling constant of 172m^{-1}, (d) reflectivity and group-delay spectra of the grating.

#190362 - $15.00 USD Received 10 May 2013; revised 4 Jul 2013; accepted 5 Jul 2013; published 15 Jul 2013

The physical significance of the features of the IS-based design can now be appreciated by comparing the coupling constants/local period variations and the reflectivities/group delay spectra, of a conventional linearly-chirped FBG [Fig. 5(c)&5(d)] and the IS-based pure 2nd-order dispersion compensator [Fig. 5(a)&5(b)). It is realized that as compared to conventional linearly-chirped FBGs, by appropriately introducing the ripples in the FBG apodization and local period variation, the IS design takes the ripples out and linearizes the group delay response. It has been understood that the group delay and the associated reflectivity ripples in conventional linearly-chirped gratings are due to residual internal "cavities" formed by spectrally partially overlapping adjacent grating sections [38]. *By introducing additional local detuning and changing the local grating coupling strength appropriately - in a mathematically rigorous way - the IS-based designs detune and reduce the spectral partial overlap of adjacent grating sections and linearize the group delay response*.

To demonstrate the aforementioned features, we have designed pure 2nd-order FBG dispersion compensators using layer-peeling IS approach and have fabricated them using the previously mentioned technique [39].

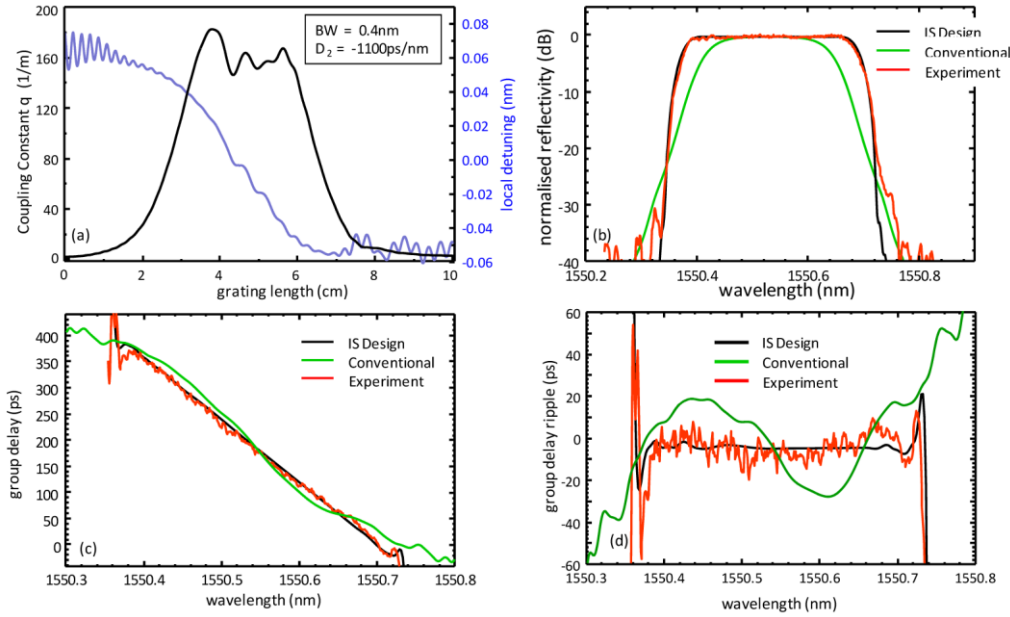

Fig. 6. (a) Coupling constant (left) and local period detuning (right) obtained with the layer-peeling IS technique, for $R_0 = 0.9$, $\Delta\lambda_0 = 0.4$nm, $m = 22$ and $D_2 = -1100$ps/nm. Theoretical and experimental (b) reflectivity spectra, (c) group delay and (d) group delay ripple (superimposed is also the reflectivity of a conventional tahn-apodized, linearly-chirped FBG with comparable reflectivity and dispersion).

The design parameters were $R_0 = 0.9$, $\Delta\lambda_0 = 0.4$nm, $m = 22$ and $D_2 = -1100$ps/nm. Figure 6(a) shows the coupling constant envelope (left) and local period detuning (right) obtained with the layer-peeling IS technique. Figure 6(b) superimposes the theoretical and experimental reflectivity spectrum, showing excellent agreement. Superimposed is also the reflectivity of a conventional tanh-apodized, linearly-chirped FBG with comparable reflectivity and dispersion [22]. It is shown that the IS design results in a much squarer reflectivity spectrum. Figure 6(c) and (d) compare the corresponding experimental and theoretical group delay and group delay deviation (ripple), respectively. It is shown that experimental data based on IS design are again in excellent agreement with theory. The low level of noise on the experimental group delay (± 10 ps peak to peak) has a very short spectral period (~10 pm) and is not expected to have a significant effect on the transmission

#190362 - $15.00 USD Received 10 May 2013; revised 4 Jul 2013; accepted 5 Jul 2013; published 15 Jul 2013

of high speed optical signals [37] [40]. The conventionally apodized, linearly-chirped FBGs, on the other hand, show substantial group delay ripples, as a result of residual internal reflections.

2.3 Pure Third-Order Dispersion Compensators ($D_2 = 0$, $D_3 \neq 0$)

The reflection coefficient of a pure 3rd-order dispersion compensator is defined by setting $D_2 = 0$ and $D_3 \neq 0$ in Eq. (8). Figure 7(a) shows the target reflectivity (left) and the corresponding group delay (right), for $R_0 = 0.9$, $\Delta\lambda_0 = 5$nm, $m = 20$ and $D_3 = -20$ps/nm^2. Figure 7(b) shows the coupling constant distribution along the fiber length obtained by applying layer-peeling IS approach. The coupling constant is real, which implies that the pure 3rd-order DC is *unchirped*. In addition, the apodization profile is super-structured with a large number of lobes with decreasing amplitude and length the further away from the main lobe. The fact that a dispersion compensating design appears to be un-chirped is a surprising and non-intuitive result.

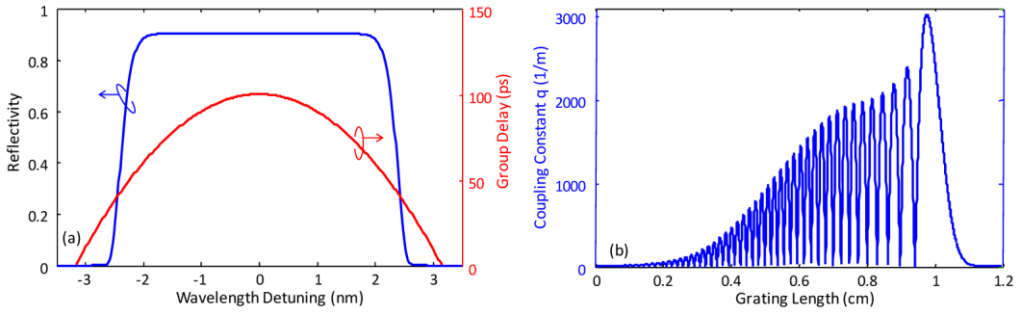

Fig. 7. (a) Reflectivity (left) and the corresponding group delay (right), for $R_0 = 0.9$, $\Delta\lambda_0 = 5$nm, $m = 20$ and $D_3 = -20$ps/nm^2, (b) coupling constant distribution along the fiber length obtained by the layer-peeling IS approach.

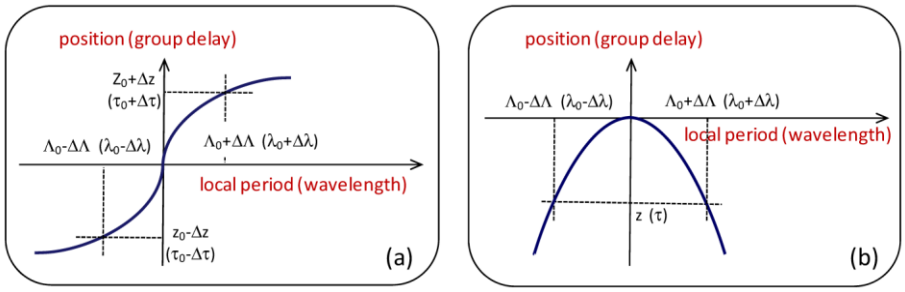

Fig. 8. Position (group delay) and local period (wavelength) interrelation schematics for (a) even-order and (b) 3rd-order DC designs.

To shed light into this apparent paradox, we first consider linearly-chirped gratings, where it is well established that the group-delay dispersion emanates from the fact that different wavelengths are reflected from different physical positions along the grating length. This is shown schematically in Fig. 8(a), where the local period (chirp) or equivalent reflected wavelength is plotted against grating position or equivalent group delay. In a monotonically varying group delay (2nd- or 4th-order dispersion) the effective reflection points are to large extent spatially separated. As can be seen in Fig. 7(a), however, in pure 3rd-order DC wavelengths placed symmetrically around the reflection bandwidth center experience the same group delay. From a physical perspective this means that they are reflected from the same position along the grating. From Fig. 8(b) it is evident that since wavelengths $\lambda_0 \pm \Delta\lambda(z)$ reflect from the same position z, the corresponding partial gratings with local periods $\Lambda_0 \pm$

#190362 - $15.00 USD Received 10 May 2013; revised 4 Jul 2013; accepted 5 Jul 2013; published 15 Jul 2013

$\Delta\Lambda(z)$ are superimposed. This superposition results in a Moiré grating with short period Λ_0 and a modulation with much longer period $\Lambda_M(z) = \Lambda_0^2/\Delta\Lambda(z)$. This eventually results in a complex grating with constant period Λ_0 throughout and a superstructure period Λ_M changing along the FBG grating. These observations provide the physical explanation of the features of the IS designs for pure 3rd-order DCs. Pure 3rd-order dispersion compensating gratings have been demonstrated experimentally [11,12].

3. Bidirectional Dispersionless FBG Designs

To overcome the uni-directionality limitations of IS dispersionless FBG designs, discussed above, modifications to the design process have been proposed. They involve fitting the target dispersion profile, utilizing a distortion functional for the group delay minimization, and using symmetry relations and IS to design symmetric FBGs [41,42]. Here we propose a simpler approach based on existing uni-directional designs and the physical insight gained from the analysis in Section 2.1. Using this insight has enabled the design and fabrication of high reflectivity (>30dB) bidirectional, dispersionless FBGs, for the first time.

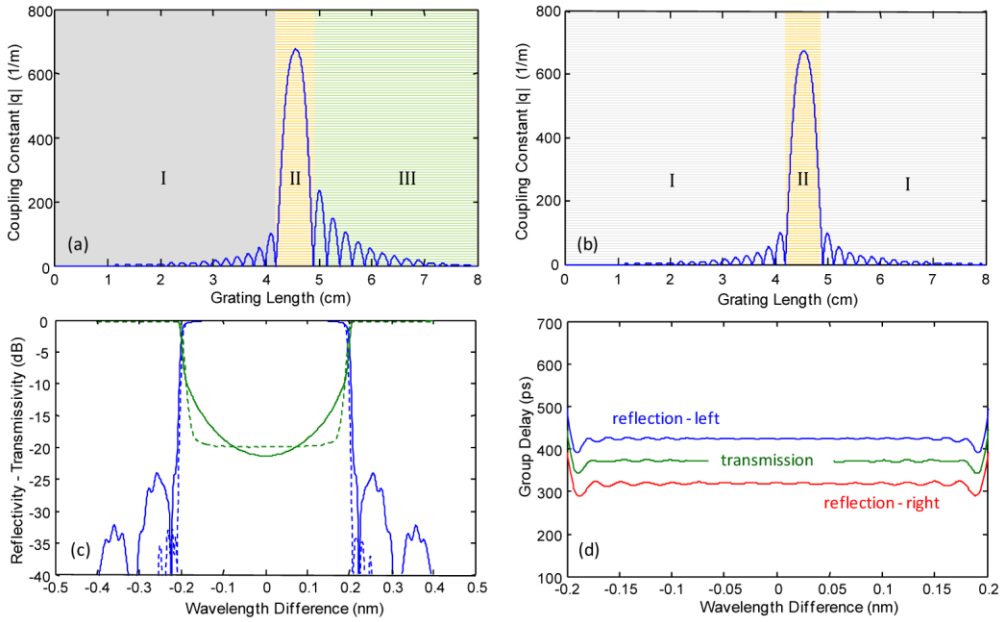

Fig. 9. (a) Unidirectional asymmetric design obtained by application of layer-peeling IS algorithm, (b) bidirectional symmetric design obtained by replacing section III by section I. (c) reflectivity and transmissivity of the symmetric (solid lines) and original asymmetric (dashed lines) designs. (d) group delays in reflection (both sides) and transmission for the symmetric design.

The starting point is the standard, unidirectional design obtained by application of layer-peeling IS algorithm, shown in Fig. 9(a). As explained in Section 2.1, section II is the main dispersive reflector while section III contributes as a small perturbation only to the reflectivity spectrum squareness, leaving the dispersion largely unaffected. On the other hand, section I provides primarily the required dispersion compensation and leaves the reflectivity spectrum almost unchanged. These observations allow us to propose the truncation of section III and its replacement with the dispersion-compensating section I. In addition, in order to make the design totally symmetric, we symmetrize the main lobe I around its center. This is a small perturbation, which does not affect the final result significantly. The resulting symmetric design is shown in Fig. 9(b). Our profile shows strong similarity with the designs obtained

#190362 - $15.00 USD Received 10 May 2013; revised 4 Jul 2013; accepted 5 Jul 2013; published 15 Jul 2013

with the much more involved design procedures discussed in the literature [41,42]. Figure 9(c) shows the obtained reflectivity and transmissivity of the symmetric (solid lines) and original asymmetric (dashed lines) designs. Compared to the asymmetric design, the symmetric design shows slightly stronger and more rounded transmission spectrum. This is a result of the truncation of part III, as discussed before in Section 2.1. Figure 9(d) shows the group delays in reflection (both sides) and transmission for the symmetric design, showing flat group delays from both sides. The group delays of the asymmetric design are similar to the ones shown in Fig. 2(c) and are not included here.

To demonstrate the bidirectional dispersionless response, we have fabricated the new symmetric designs using the modified "moving fiber-scanning beam" technique [35,36]. The symmetric profile is shown in Fig. 10(a) (red line). It should be stressed that these IS-based symmetric profiles are considerably different to sinc profile, which are known to provide bidirectional dispersionless response only at low reflectivities (<~10%). In Fig. 10(a) we have also included the sinc profile (blue line) with the same main lobe, for comparison. Figure 10(b) and 10(c) show the corresponding design and experimentally obtained reflectivities and the group delays from both sides. It is shown that our symmetric design gives almost identical dispersionless response from both sides, in excellent agreement with theory.

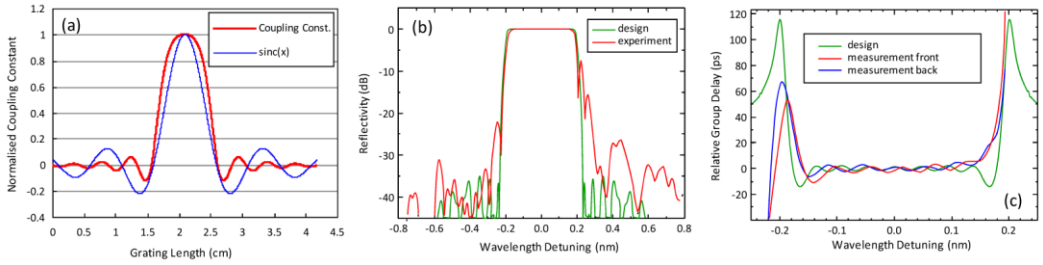

Fig. 10. Dispersionless bidirectional FBG (a) normalized coupling constant profile (red line) and sinc profile (blue line) ((b) reflectivity (design – green & experiment - red) and (c) time delay from front (red), back (blue) sides and design (green).

4. Summary - Conclusions

We have revisited some of the most successful IS FBG designs and, for the first time, we have shed physical insight into their coupling constant profile, as well as, their reflectivity characteristics. We first demonstrated numerically and experimentally that dispersionless, square FBG filters are actually *dispersion compensated* devices and we physically identified the spatially separated *main (dispersive) reflector* and *dispersion compensator* sections. We also looked into the features of pure 2nd-order dispersion and 3rd-order dispersion compensator designs and discussed their physical importance. We showed that their non-intuitive apodization profile features can be explained using fundamental physical arguments. Finally, we have used this knowledge to design and fabricate for the first time strong (>30dB) bidirectional gratings with dispersionless response from both sides, suitable for simultaneous add AND drop functions out of the same device.

Acknowledgements

This work was partially supported by the EPSRC Center for Innovative Manufacturing in Photonics, University of Southampton, UK.

#190362 - $15.00 USD Received 10 May 2013; revised 4 Jul 2013; accepted 5 Jul 2013; published 15 Jul 2013